



Water effects on urban heat islands in summer using WRF-UCM with gridded urban canopy parameters — A case study of Wuhan

Dun Zhu^a, Xuefan Zhou^{a,*}, Wei Cheng^b

^a School of Architecture and Urban Planning of Huazhong University of Science and Technology, China

^b Wuhan Land Use and Urban Spatial Planning Research Center (WLSP), China



ARTICLE INFO

Keywords:

Urban heat islands
Water body
Ventilation channel
WRF-UCM
Urban canopy parameters (UCPs)

ABSTRACT

Urbanization has rapidly occurred in China along with a significant reduction in ecological resources, greatly exacerbating urban heat island effect. In cities with abundant inland lake resources, it is valuable to study the use of climate regulation effects of water bodies to improve the urban climate environment. In this study, we built a single-layer urban canopy model with higher accuracy by importing gridded urban canopy parameters and studied the impact of water bodies distributed in different areas of Wuhan on the urban thermal environment using a weather research and forecasting model (WRF). Water bodies located in the upwind suburbs had the greatest cooling impact on the microclimate of downtown areas during the day. Furthermore, they promote the evacuation of heat inside the urban canopy to the upper air by enhancing the lake breeze circulation. Late morning temperatures drop above the ground when the breeze circulation fully develops, while the temperature rise in the upper air increases. However, the cooling effect of these water bodies on the downtown area was affected by construction intensity in the suburbs. When the building density increased from 20% to 40%, the cooling effect did not change significantly. However, a further increase from 40% to 60% increased the proportion of intense heat island areas downtown, and the cooling effect of water bodies was also severely weakened. Moreover, with an increase in building density in the suburbs, the intense heat island areas north of the city gradually expanded to the city center.

1. Introduction

Economic growth has contributed to rapid urbanization in China. However, a lack of scientific planning has led to an increase in building density and substantial damage to natural environments, which in turn cause serious urban heat islands and air pollution issues [1]. Urban ventilation channels that rely on ecological resources should be built to promote urban ventilation and alleviate urban climate problems [2,3]. However, the options are based on the generalized ventilation channel theory proposed by Kress in 1979, including the affected space (Wirksungsraum), compensation space (Ausgleichsraum), and air duct (Luftleitbahn) [4]. The core mechanism is to take the compensation space, usually forest or wetland, as the source of cold air migration and to adjust the climate of urban areas as the affected space.

Waterbodies can improve the urban thermal environment as excellent ecological compensation spaces. The large thermal inertia and capacity, as well as the low thermal conductivity and radiation rate, qualify it as an urban cold island, which is more effective than other

underlying surfaces such as farmland and woodland in mitigating urban heat islands [5,6]. Moreover, in the lower atmosphere, the lake wind circulation triggered by the lake-land temperature difference can not only promote the vertical evacuation of accumulated urban heat and air pollution, but also change the structure of the heat island circulation [7,8]. Yang et al. analyzed the relationship between the lake breeze circulation brought by Taihu Lake, urbanization process of Suzhou, and urban heat island circulation using the regional boundary layer model (RBLM) [9]. The lake breeze reduced the height of the mixed layer in Suzhou City by 300 m during the day and played a significant role in alleviating the increase in surface turbulent kinetic energy and sensible heat flux caused by urbanization, indicating that the development of heat island circulation is inhibited.

The ability of a water body to regulate the climate is affected by many factors. First, its influential ability increases significantly with an increase in surface area and water storage capacity [10]. Through remote sensing inversion, Wu et al. found that the cooling intensity increased logarithmically with an increase in wetland area, and the

* Corresponding author.

E-mail addresses: m201877353@hust.edu.cn (D. Zhu), xuefanzhou@hust.edu.cn (X. Zhou), chengwei@wlsp.org.cn (W. Cheng).

threshold of efficiency was 1.47 ± 0.34 ha [11]. The shape characteristics of the water bodies also have a significant impact on the cooling and humidifying abilities of wetlands. Ji et al. [12] found that irregularly shaped wetlands had the greatest cooling and humidifying abilities, followed by regular-shaped wetlands (near circular wetlands, near rectangular wetlands) and strip-shaped wetlands. Second, spatial relationships such as the distance between the water body and urban areas significantly affect the climate regulation ability of the water body. As mentioned in our previous study, downtown lakes have the greatest influence on the climate of downtown Wuhan, nearby suburban lakes less so, and more distant suburban lakes even less [13]. Through computational fluid dynamics (CFD) simulations, Liu et al. (2019) found that when a lake is close to or far away from a city, lake breeze circulation and urban heat island circulation have synergistic and antagonistic effects, respectively [14]. In general, water bodies have the most significant climatic impact on urban areas when they are located upwind. In a study of high-temperature weather with southerly winds, Xia et al. found that Taihu Lake had the most significant cooling effect on Wuxi City in the north, and the maximum cooling range in the boundary layer could reach $0.5\text{--}0.7$ °C. For Suzhou on the east side, the maximum temperature drop in the boundary layer was $0.2\text{--}0.3$ °C [15]. This azimuthal relationship also affects the formation and development of lake breeze circulation. When the background wind direction is offshore, with the wind blowing from the urban land to the lake surface, the temperature gradient between the lake and land will further increase, which is more conducive to driving the lake breeze circulation generated by the thermal difference; otherwise, it will have an inhibitory effect [16]. However, strong offshore winds can hinder the lake breeze from advancing inland, and if it is strong enough (usually more than 5 m/s), the lake breeze front can be prevented from coming ashore or forming [17].

As an affected space, the construction of urban areas also significantly impacts the climate regulation ability of water bodies. When water bodies are located inside an urban area, the area also acts as an air channel, which determines the extent to which the compensation space can extend. Ji et al. observed four lake wetlands in Daqing, China, and found that the cold island effect is greatest in urban center wetlands, followed by suburban wetlands 1 (higher construction intensity), suburban wetlands 2 (lower construction intensity), and, lastly, outer suburban wetlands [18]. Wu et al. concluded, using a regression model, that there is a negative correlation between the distance from water bodies to the urban center and the cold island effect ($R_s = -0.608$) [19]. These results indicate that the increase in construction intensity increases the urban temperature and the lake-land temperature difference, which may make the cold island effect of the water body more pronounced. However, this improvement is not unlimited. If the damage to the climate regulation capacity caused by the shrinking wetland area and deterioration of water quality caused by urban expansion is not considered, overly dense buildings will also lead to weakening of lake and sea breeze penetration, which is quite unfavorable [20]. Cheng et al. conducted several numerical experiments using a weather research and forecasting model (WRF) with urban construction status in 1988, 1999, and 2010 as the lower boundary condition. The results show that, although urbanization increases the duration and intensity of sea breezes, it significantly hinders inland infiltration. From 1988 to 2010, the sea breeze boundary moved back by approximately 4 km, and because the urban area in the region is concentrated near the coast, urbanization created a negative heating gradient for the farther inland areas, which may hinder the propagation of sea breezes [21]. Hong et al. studied the influence of the block spatial form on both sides of the Yangtze River in Wuhan on the infiltration of river breezes based on field measurements combined with CFD simulation. They found that when the street direction was parallel to the wind direction, blocks with a high degree of enclosure were conducive to the infiltration of the river breeze, and when the wind direction was at an angle of $22.5^\circ\text{--}45^\circ$ to the street, the river breeze infiltrated smoothly in blocks with a low enclosure degree [22].

Therefore, for cities with abundant marine or inland lake resources, carrying out urban planning around water bodies to maximize their climate regulation ability of water bodies is of great significance for sustainable development.

In recent years, the use of natural resources, such as water, to realize scientific urban planning through simulation experiments has been explored. Among them, mesoscale meteorological simulation software, namely the Weather Research and Forecasting Model (WRF), is widely used owing to its suitable scale and good coupling of the urban canopy model (UCM), hydrological, and chemical models. Using a single-layer urban canopy model in WRF, Miao et al. assessed the impact in climate of urban hydrological processes such as evaporation from impervious surfaces, urban irrigation, and urban "Oasis Effect" in Nanjing, China [23]. In urban planning, WRF-UCM is often used to predict and evaluate the effectiveness of urban ventilation channels to ensure the scientific nature of engineering [24,25]. However, as a mesoscale meteorological simulation tool, the insufficient urban model is an obvious shortcoming of WRF-UCM, in which urban land can only be divided into three types [26], addressed with the release of the National Urban Data and Access Portal Tool (NUDAPT) by the U.S. Environmental Protection Agency (US EPA). The urban canopy parameter (UCPs) dataset in NUDAPT grids builds data into $1\text{ km} \times 1\text{ km}$ horizontal grids and calculates the urban form indicators of 44 US cities, which can be directly used in the calculation of UCM [27,28]. This dataset can assign independent urban morphological parameters to each WRF computing grid, thereby improving the accuracy of urban climate simulation. To date, this dataset has been widely used in research [29–31]. If the purpose is only to estimate the air temperature at 2 m above the ground, a simple scheme would be acceptable to meet this requirement. However, if urban heat island mitigation strategies or urban-scale air-conditioning energy consumption are to be assessed, complex urban canopy schemes and detailed UCPs are essential [32]. In summary, building a WRF-UCM model based on the UCPs dataset provided by NUDAPT is an excellent way to study the effects of water bodies on urban climate regulation, particularly in highly developed cities.

Although relevant research on the impact of urban water bodies on urban climate has been conducted, most of the current research is undertaken by meteorological researchers, and the objects are mostly the macro-level impacts of oceans or large inland water bodies on cities. However, in most inland cities, there are no oceans or large lakes; instead, numerous small and medium-sized lakes are scattered around the city. In this case, a research method that treats water bodies and urban areas as two independent objects is not applicable. For example, in Wuhan City, one of the megacities with the most abundant wetland resources in inland China, there is a water surface area of 2217.6 square kilometers, accounting for 26.1% of the total urban area. In addition to the Yangtze River, the longest river in Asia that runs through the city, Wuhan also has 166 small- and medium-sized lakes, which are widely distributed inside and outside the city. When a city expands, it will inevitably cause damage to natural resources such as wetlands and woodlands in the suburbs [33,34]. Therefore, it is necessary to divide water bodies geographically and build an urban-hydrological model to evaluate the climate impact of suburban water bodies in different urban locations to determine the optimal direction of future urban expansion. Second, the focus is mostly on the impact of single or multiple wetland spaces on their surrounding microclimate, and attempts to explore how to control the block spatial form of the waterfront area to exert the cold island effect of the water body [35–37]. These studies systematically evaluated the quantitative relationship between various attributes of water bodies and their climate regulation capabilities, and provided scientific guidance for block-scale waterfront construction. However, macro-quantitative construction strategies at the urban scale are lacking. For example, when planning the construction or expansion of urban areas, controlling the construction intensity indicators and maximizing the protection and utilization of ecological resources are urgent problems to be solved. Third, in terms of simulation tools, although a more

refined urban model can be established based on NUDAPT, it only provides data for 44 cities in the US. Thus, Chinese cities urgently need to build their own UCPs datasets to realize the diverse descriptions of urban forms in the WRF. The building vector data in the center of Xi'an were successfully meshed and imported into the urban canopy model for calculation, which proved to be accurate [38]. This indicates that the proposed method is applicable to Chinese cities. Therefore, establishing a UCPs dataset is urgently required to improve the level of urban climate simulation research in China.

Therefore, this study considers the Chinese city of Wuhan as the research object and uses WRF coupled with the urban canopy model as a method to study the impact of water bodies distributed in different regions on the thermal environment of the downtown area during hot summers. Through this study, we aim to address the following three questions: ① create a UCPs dataset in the downtown area of Wuhan, build a WRF-UCM model based on this, and test whether it improves the accuracy of urban climate simulation; ② divide the suburbs into several parts according to the prevailing wind direction in Wuhan in summer, and evaluate the capacity of water bodies in each area to affect the thermal environment of the downtown area; ③ predict how the climate regulation capacity of suburban water bodies will be affected when the construction intensity increases, which will produce the value for building density and height. This study aimed to quantify the capacity of widely distributed small- and medium-sized water bodies in Wuhan to affect the urban microclimate in summer and provide a scientific reference for future urban planning. It provides a new perspective for solving urban climate problems by optimizing the urban layout and making full use of the ecological regulation of existing water bodies. The regional division method adopted in this study can also be used as a reference for other cities with abundant inland lake resources. In addition, more accurate predictions of the urban thermal environment are obtained by using the UCP-based urban canopy model established in this study. In the case of other cities, the same method can be used to create more accurate simulations of the local urban climate.

2. Methodology

2.1. WRF nested domain and boundary condition settings

The modeling system used in the current study was the WRF version 3.9. The horizontal domain was composed of three two-way nested domains with 71×71 (4.5 km), 91×91 (1.5 km), and 109×109 (0.5 km) grid points (Fig. 1, Table 1). The largest domain (D01) covered most of Hubei Province, whereas D02 and D03 included Wuhan City and downtown, respectively. Each domain had 39 unevenly spaced full sigma layers in the vertical direction, 16 of which were less than 2 km long.

Meteorological initialization field data were obtained from the National Centers for Environmental Prediction Final Operational Global Analysis (NCEP-FNL) dataset. The Operational Model Global Tropospheric Analyses data included a $0.25^\circ \times 0.25^\circ$ grid prepared operationally every 6 h. The original data for land use and land cover were obtained from the United States Geological Survey (USGS), with a spatial resolution of $30 \text{ s} \times 30 \text{ s}$ for D01 and D02, while that for D03 was obtained from the GlobalLand30 dataset with a geographic resolution of 30 m (<http://www.globalandcover.com/GLC30Download/index.aspx>) [39].

The selected physical parametrization schemes are presented in Table 2. To accurately show the urbanization of Wuhan, the parameter input of the single-layer UCM module was obtained from documents provided by the Wuhan Municipal Planning Bureau (<http://zrzhgj.wuhan.gov.cn/>). Furthermore, this study replaced the ideal parameterization scheme of urban morphology in the conventional UCM model with UCPs to improve the simulation accuracy of the WRF in urban microclimates by refining the urban model. The UCPs dataset was calculated based on the 2018 vector building data in Wuhan, and the

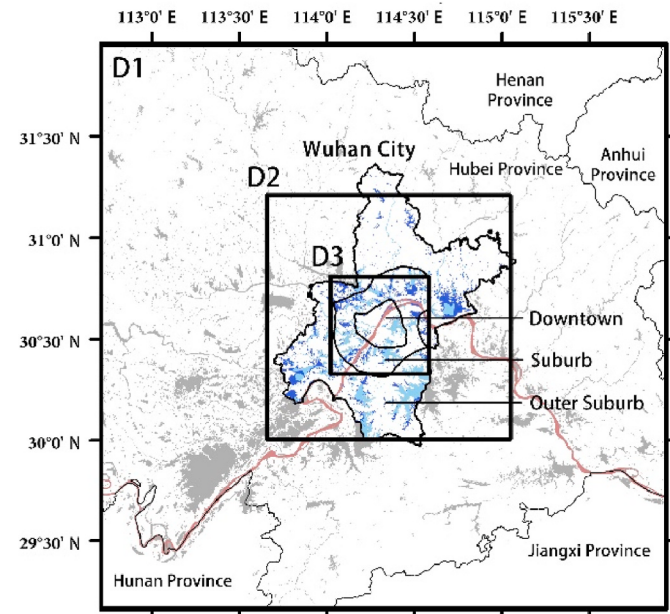


Fig. 1. Nested Domain setting.

Table 1
Nested domain grid number and spacing.

	Domain (X[km] × Y[km] × Z[km])	Number of grids	Grid size (km)
D1	$315 \times 315 \times 20$	$70 \times 70 \times 39$	4.5
D2	$135 \times 135 \times 20$	$90 \times 90 \times 39$	1.5
D3	$54 \times 54 \times 20$	$108 \times 108 \times 39$	0.5

Table 2
WRF physical scheme selection.

WRF physics suite	D1	D2	D3
Microphysics	Lin et al.	Lin et al.	Lin et al.
Cumulus	Kain-Fritsch (new Eta)	/	/
Longwave radiation	RRTMG	RRTMG	RRTMG
Shortwave radiation	Goddard	Goddard	Goddard
Boundary layer	YSU	YSU	YSU
Surface layer	Revised MM5	Revised MM5	Revised MM5
Land surface	Noah LSM	Noah LSM	Noah LSM
Urban Surface	/	/	SLUCM
Lake model	CLM 4.5	CLM 4.5	CLM 4.5

geographical resolution was $0.33 \text{ km} \times 0.33 \text{ km}$. The appendix briefly introduces the data flow of the UCPs in the UCM and the construction process of the UCPs dataset in Wuhan.

2.2. Model validity verification

To compare the results of the UCP-based model with those of the conventional UCM model, we conducted a 37-day simulation for four consecutive periods in the summer of 2015: July 6–12, July 17–21, July 29–August 6, and August 20–September 4. The simulation experiment avoided continuous rainy weather conditions. In addition, the focus of this study was to achieve an accurate short-term prediction of the thermal environment within the urban canopy under high-temperature weather. In other words, we focused on the response of the air temperature results of the model as the solar radiation changes during the day. However, because the background climatic conditions vary from day to day, the diurnal trend in temperature averaged over a longer period is relatively smooth, making it difficult to detect changes. Therefore, we also recorded and analyzed the simulation results from

0:00–24:00 (UTC+8) on August 22 (high temperature and sunny day).

We built three urban models: NOUCM (the default slab model in WRF without calling the urban canopy model), 3UCM (using the conventional single-layer urban canopy model), and UCPS (using gridded UCPs and frc_urb data). The simulation results of the air temperature at 2 m above the ground (T2) and the surface temperature (TSK) of each model at 14:00 (UTC+8), August 22, are shown in Fig. 2.

The spatial difference in T2 in NOUCM was insignificant (Fig. 2a–c) and hardly reflected the thermal environment differences caused by the diversity of urban morphology in different regions. The difference between the simulation results of the 3UCM and NOUCM was not significant. Although the UCPS model performs well, areas with harsh thermal environments inside the city can be identified so that the ventilation in these areas can be focused on urban development. From Fig. 2d–f, the spatial difference in the surface temperature was more obvious. However, the slab model treats the entire city as a homogeneous plane; hence, the simulation shows that the surface temperature of the underlying urban surface is stable everywhere. For urban studies, the prediction accuracy is unacceptable. Although the results of the 3UCM are good, there are only three different urban parameters; hence, there is homogenization, as the simulation results can approach UCPS only

when there are sufficient city classifications. Therefore, UCPs-based models have significant advantages in terms of reflecting thermal differences caused by urban morphological diversity.

To test the accuracy of the models, the simulation results from 0:00–24:00 (UTC+8) on August 22 (a total of 25 h) were compared with the observation results obtained at the Wuhan Meteorological Bureau stations. In addition, the 37-day simulation results, as well as the corresponding observations, were presented as the average temperature for each hour in the day. The temperature at a single hour in each day (e.g., the temperature at 9:00 a.m. for each of the 37 days) was added together and divided by 37 to obtain the average temperature at 9:00 a.m.; similarly for 10:00 a.m. and so on. The result is 24 data points, each one representing the average temperature of a particular hour in the day, named 37-day mean. The air temperature at 2 m above the ground (T2) is shown in Fig. 3 and Table 3. The three stations included Jin Yin Lake (JYL), located in the suburbs ($114^{\circ}13'47''$ E, $30^{\circ}40'12''$ N); Hong Gang Cheng (HGC), ($114^{\circ}23'59''$ E, $30^{\circ}38'24''$ N), and Liang Dao Street (LDS), located in the downtown area ($114^{\circ}18'36''$ E, $30^{\circ}32'59''$ N). The HGC site is characterized by low-rise residences; in contrast, the LDS site is much more developed, in terms of both commerce and population flow.

By comparing the results of the single-day and 37-day means, it can

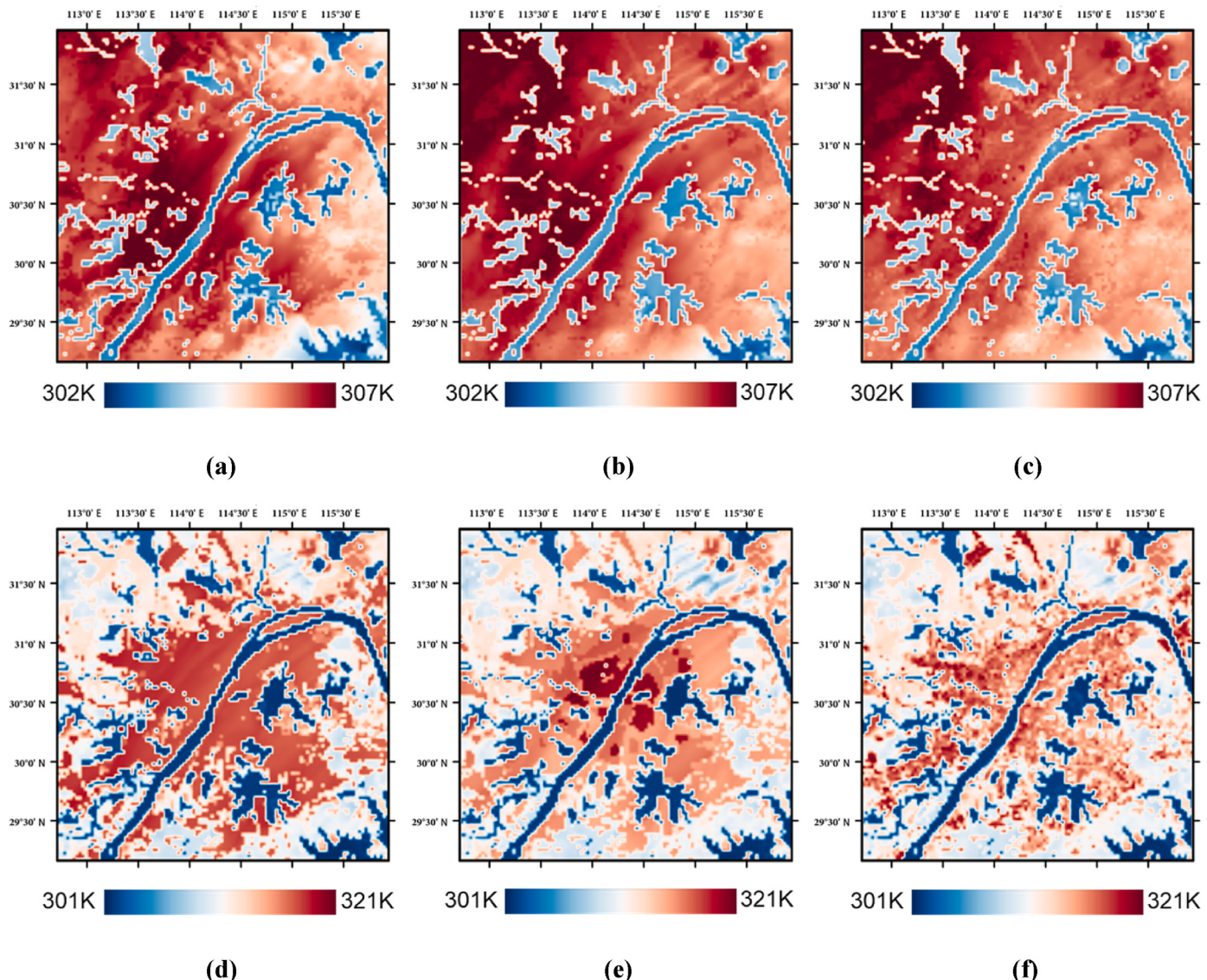


Fig. 2. Air temperature 2 m above the ground (T2) and surface temperature (TSK) at 14:00 (UTC+8), August 22, in different simulations (described in the text): (a) NOUCM T2, (b) 3UCM T2, (c) UCPS T2, (d) NOUCM TSK, (e) 3UCM TSK, 14:00 (f) UCPS TSK.

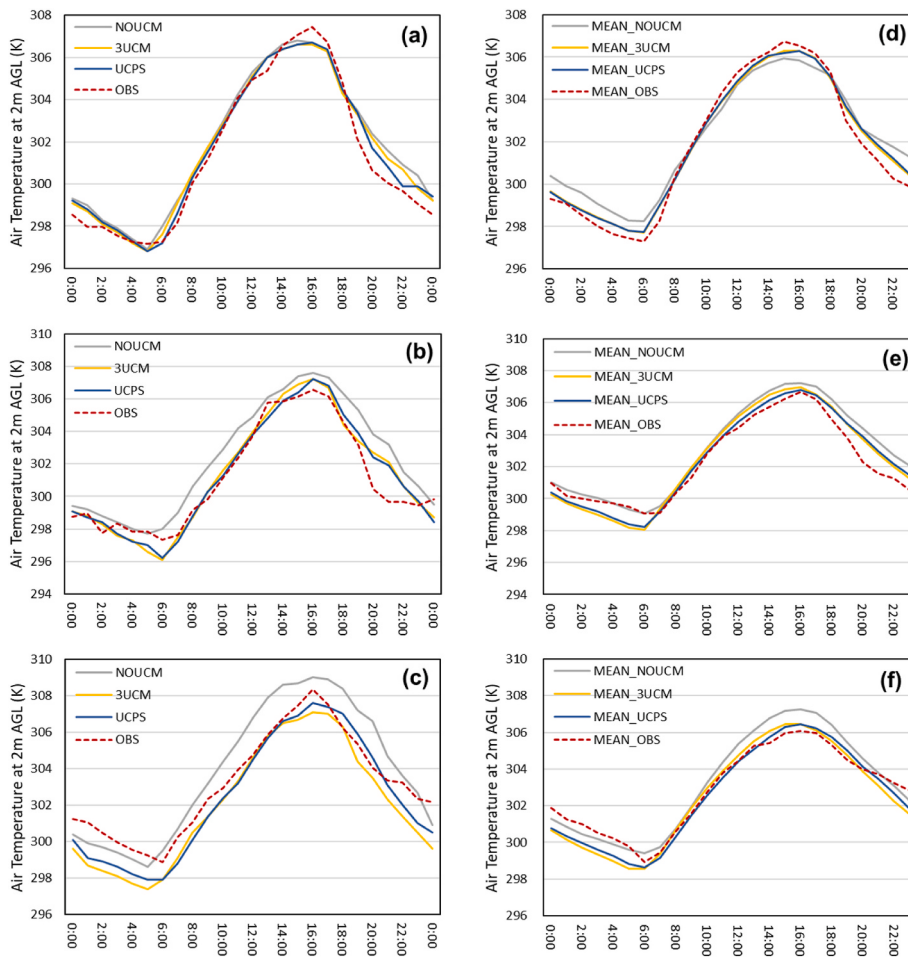


Fig. 3. Comparison of simulation and observation results obtained by meteorological stations, T2. (a) Jin Yin Lake, August 22, (b) Hong Gang Cheng, August 22, (c) Liang Dao Street, August 22; (d) Jin Yin Lake, 37-day mean, (e) Hong Gang Cheng, 37-day mean, (f) Liang Dao Street, 37-day mean.

Table 3
Verification of temperature on August 22 and 37-day mean.

T2 (K)	24H AVERAGE		MB Mean	MB Mean	RMSE Mean	RMSE Mean	R	R Mean
	OBS	OBS Mean						
JYL	NOUCM	301.27	301.81	0.55	0.35	0.97	0.85	0.976**
	3UCM			0.38	0.13	0.88	0.43	0.975**
	UCPS			0.34	0.15	0.78	0.46	0.981**
HGC	NOUCM	301.12	302.31	1.20	0.73	1.53	0.96	0.960**
	3UCM			0.17	0.20	0.91	0.78	0.967**
	UCPS			0.13	0.17	0.86	0.71	0.969**
LDS	NOUCM	303.13	302.85	0.72	0.36	1.33	0.72	0.973**
	3UCM			-1.13	-0.30	1.34	0.74	0.983**
	UCPS			-0.75	-0.29	1.03	0.59	0.987**

Note: MB is the difference between the 24-h average of the predicted and observed values. RMSE is the root-mean-square error. R is Pearson's correlation coefficient. ** Correlation is significant at the 0.01 level (2-tailed).

be seen that the relationship between the prediction results of each model and the observations is basically the same (Fig. 3, Table 3). However, in the case of the 37-day mean results, owing to the averaging of different background meteorological conditions, the error values are relatively small, and the trend in the change in air temperature changes with time (within 24 h) is also smoother. Then, in Fig. 3 (a) and (d), the results show that the differences between the three models are not significant for JYL, which is in good agreement with the monitoring data. This is mainly because suburban construction intensity is low; therefore, the urban model used has no significant impact on the simulation

results. However, the rate of temperature decrease and the average temperature after sunset in all models were significantly higher than those observed. This is because thermal parameters, including anthropogenic heat emissions and building heat capacity, were not included in the UCPS dataset but were input by URBPARAM.TBL according to the three classifications. Therefore, higher numerical settings in suburban areas may lead to higher evening temperatures. However, the deviation of UCPS values from actual observations is still minimal (~ 0.5 K) = , whereas NOUCM is generally above 1 K, both in the single-day and 37-day results.

For the two sites located downtown (HGC, LDS), both the deviation and correlation coefficients of the 3UCM and UCPS cases using the urban canopy model were significantly higher than those of NOUCM. The values generated by NOUCM deviated greatly from the observed values; the model overestimated the temperature in the HGC and LDS during the day, with a deviation of up to 2 K during both the daytime and nighttime. The results of the UCPS-based model were closest to the observed values, with a deviation of only 0.17 K and -0.29 K (37-day mean, Table 3). The lowest RMSE and highest correlation were obtained with the UCPS-based model. It can also be seen in Fig. 3 (b), (c), (e), and (f) that, during the day, the gap between the UCPS predicted values and observations is also the smallest. However, both urban canopy models underestimated the nighttime temperatures by approximately 1 K. This may be related to inaccurate anthropogenic heat estimates, as the significant increase in local air temperature caused by the intensive use of air conditioners in the summer was not considered. Overall, the model based on UCPS + frc_urb had the highest accuracy for urban temperature simulations and was suitable for microclimate research in Wuhan. Therefore, this method was used to conduct sensitivity experiments.

2.3. Case setting for sensitivity experiments

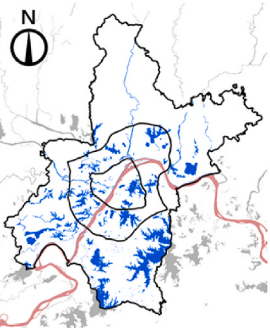
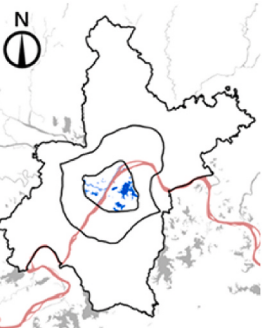
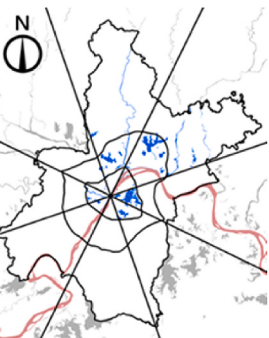
The purpose of the first part of this study is that there are many lakes distributed in the suburbs of Wuhan, and we hope to explore the relationship between the impact of water bodies on the downtown thermal environment and their location. Therefore, we used the UCPS-based single-layer urban canopy model to conduct sensitivity experiments using the various case settings listed in Table 4. The nested regions, physical schemes, and boundary condition settings for all the cases were consistent with those described in Section 2.4. By modifying the land use category in the WRF Preprocessing System (WPS), we can replace water bodies in specific areas with dry land (U.S. Geological Survey Category

2). Thus, the impact of these water bodies on climate can be reflected individually. The NL case was used as the control group, and all water bodies in Wuhan, except for the Yangtze River, were replaced with dry land. After subtracting the results of the control group from those of the experimental group, the obtained value was the effect of water bodies on the climate. As this experiment mainly focused on the interaction between water bodies, dominant wind direction, and urban area, we designed four sets of experimental cases. The dominant wind direction in Wuhan in summer is southwest; hence, the three are as follows: ① only water bodies in downtown and suburban water bodies in the southwest direction (i.e., those located upwind of downtown) are preserved, named UP; ② only water bodies in downtown and suburban water bodies in the northeast direction (i.e., those located downwind of downtown) are preserved, named DOWN; ③ only water bodies in downtown and suburban water bodies on the east and west sides are preserved, named SIDE.

As the water bodies in downtown areas have been strictly protected by law, it is impractical to preserve only suburban water bodies and remove those in downtown areas. Moreover, our previous research concluded that there should be a synergistic effect between water bodies in the suburbs and downtown areas, thereby enhancing climate regulation capacity [13]. Therefore, in these three cases, water bodies in the downtown area were preserved. Furthermore, in DL, water bodies in downtown areas are preserved, whereas those in suburbs are replaced by dry land. By comparing DL with the above three cases, the capacity of suburban water bodies to influence the climate can be determined.

In this study we focused on the impact of water bodies on the urban thermal environment, considering that the thermal difference between the lake and land is greatly affected by the background temperature, wind speed, and direction, which also directly affect the formation and development of the lake-land breeze. To explore the details of this effects, we utilized short-term studies for a single background

Table 4
Case setting.

Real	NL	DL
 Real situation, not for simulation	 Remove all water bodies in the city	 Retain water bodies in downtown
UP  Retain water bodies in downtown and upwind area	SIDE  Retain water bodies in downtown and both sides	DOWN  Retain water bodies in downtown and downwind area

Note: The river marked in red is the Yangtze River and has not been replaced in any case.

meteorological condition. In addition, as stated in Section 2.2, the optimization of the model is mainly aimed at the response of the air temperature prediction results as the solar radiation changes during the day. Therefore, in this study, dates with typical summer weather conditions in Wuhan were selected for the simulation experiments.

To find the most representative simulation time period, we reviewed the historical meteorological data from 2016 to 2019; the wind frequency and high temperature days (maximum temperature $>35^{\circ}\text{C}$) are shown in Fig. 4. The following two factors were considered when selecting the simulation period: ① continuous high temperature, sunny, and without heavy clouds; ② wind direction during the simulation was the dominant wind direction in Wuhan in summer - the southwest. Taking the above factors into consideration, we chose July 25–28, 2016, as the period in which to conduct a total of 72 h of short-term simulation, and the results from July 27 between 0:00 and 24:00 (UTC+8) were considered for the analysis.

3. Results

3.1. Impact of water bodies on the thermal environment above ground

In this section, we explore and evaluate the capacity of suburban water bodies distributed upwind, along the sides, and downwind of downtown areas to influence the microclimate downtown during hot summers. Fig. 5 shows the difference in T2 (air temperature at 2 m above ground) and V10 (wind speed at 10 m above ground) between the experimental cases (DL, UP, SIDE, DOWN), and control case NL (results of experimental case-control case), which reflects the spatial distribution characteristics of the impact of water bodies on the urban thermal environment. To make it easier to identify the water bodies that were preserved in each case, lines used to delineate the orientation (dashed black lines) were added.

Comparing Fig. 5a and b, it can be seen that at noon, when solar radiation and air temperature are high, the additional cooling effect of upwind water bodies is the most significant. In the southern part of downtown, the additional cooling can reach 0.4 K, while it is slightly lower in the northern part, but there is also a decrease of 0.2 K in most areas. This is because the southwesterly wind carries cool air over upwind waterbodies downtown. From Fig. 5c and d, the cooling effect of the suburban east-west side water bodies downtown is weaker, whereas only the western edge is slightly affected. DOWN showed no difference compared with DL. In addition to the inflow of cool air, water bodies also affect air movement, and hence, the evacuation of urban heat. The horizontal wind speed difference plots in Fig. 5 (a1)–(d1) show that water bodies significantly enhance the wind speed in the downwind area

of the city, with an increase of 0.4–0.8 m/s, and areas where the wind speed increases coincide with the area where the air temperature decreases significantly, as shown in Fig. 5a–d. In addition, in Fig. 5(a1)–(d1), the wind speed difference generally presents a negative value over the preserved water bodies, which means that there should be an attenuation effect on horizontal wind speed. According to circulation theory, this may be caused by the lake breeze, which partly converts the horizontal background wind to the vertical direction, causing the heat near the ground to evacuate to the upper air (discussed using the vertical section diagram in Section 3.2).

Compared with dry land in the control experiment, the thermal inertia of the water body was much larger; therefore, in the process of the disappearance of solar radiation at night, the temperature of the water surface and air above the water surface decreased significantly lower than that of dry land. Therefore, compared with the control group, water bodies may increase the air temperature in downtown areas, especially in areas around the water body. However, the result shows that downtown water bodies only raise the air temperature above themselves, but bring a cooling effect of 0.4–0.8 K in most downtown areas (Fig. 5e), which is even more pronounced in the eastern area where water bodies are more abundant. This is not contrary to the theory but because the heat acquisition of urban areas throughout the day is an accumulation process. As shown in Fig. 5a–d and 5(a1)–(d1), water bodies significantly reduced the urban air temperature during the day and promoted the evacuation of heat, which in turn reduced urban heat accumulation during the day. The results show that for water bodies in downtown areas, the reduction of heat accumulation by the cooling effect during the day is significantly greater than the warming effect in the evening, at least for a few hours after sunset. Hence, in the evening hours, when the intensity of the urban heat island is high, downtown water bodies may mitigate rather than exacerbate this phenomenon.

Regarding suburban water bodies at night, Fig. 5f-(h) show that comparing DL with the other three cases, the cooling effect of the water body is $DL \geq DOWN > SIDE > UP$. As water bodies in downtown areas show a cooling effect, which is significantly weakened when acting together with suburban water bodies, the warming effect of suburban water bodies at night is greater than the cumulative cooling effect during the day. This is consistent with the pattern found during the day, where the evening southwesterly wind carries warm air over water bodies in the upwind suburbs to downtown. In Fig. 5f, suburban water bodies located upwind of downtown transport the most significant warming at night, almost offsetting the cooling effect of downtown water bodies. Although suburban water bodies can weaken the cooling effect of those in downtown areas, their combined effect still plays a positive role in the mitigation of urban heat islands at night. In addition, from the wind

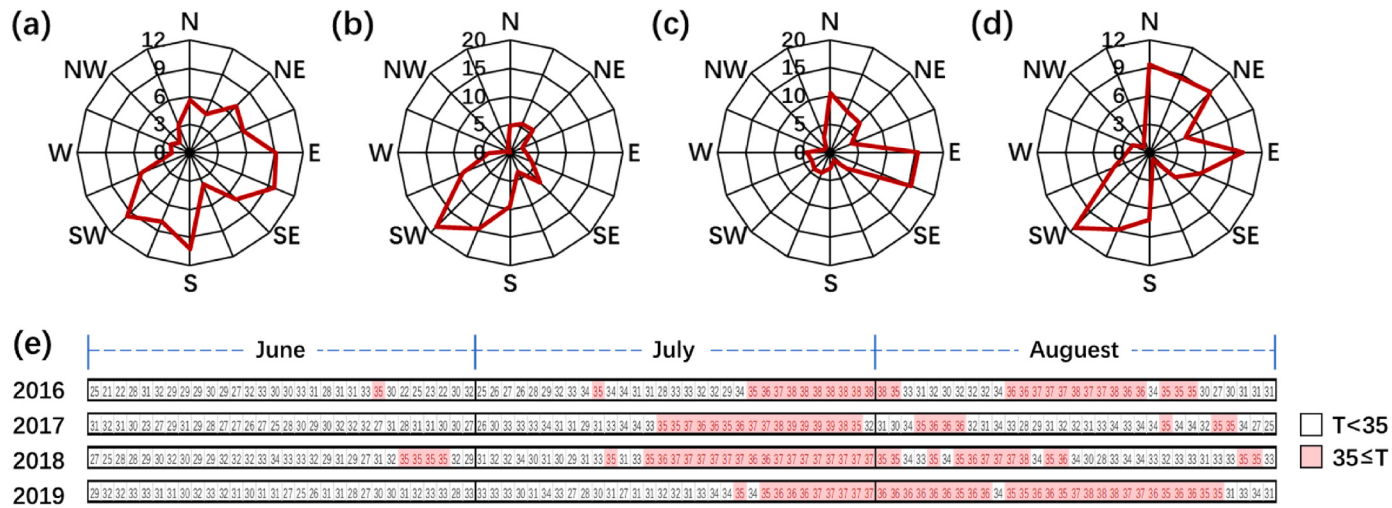


Fig. 4. Wind rose and daily maximum temperature in June–August 2016–2019. (a) 2016, (b) 2017, (c) 2018, (d) 2019, (e) daily maximum temperature.

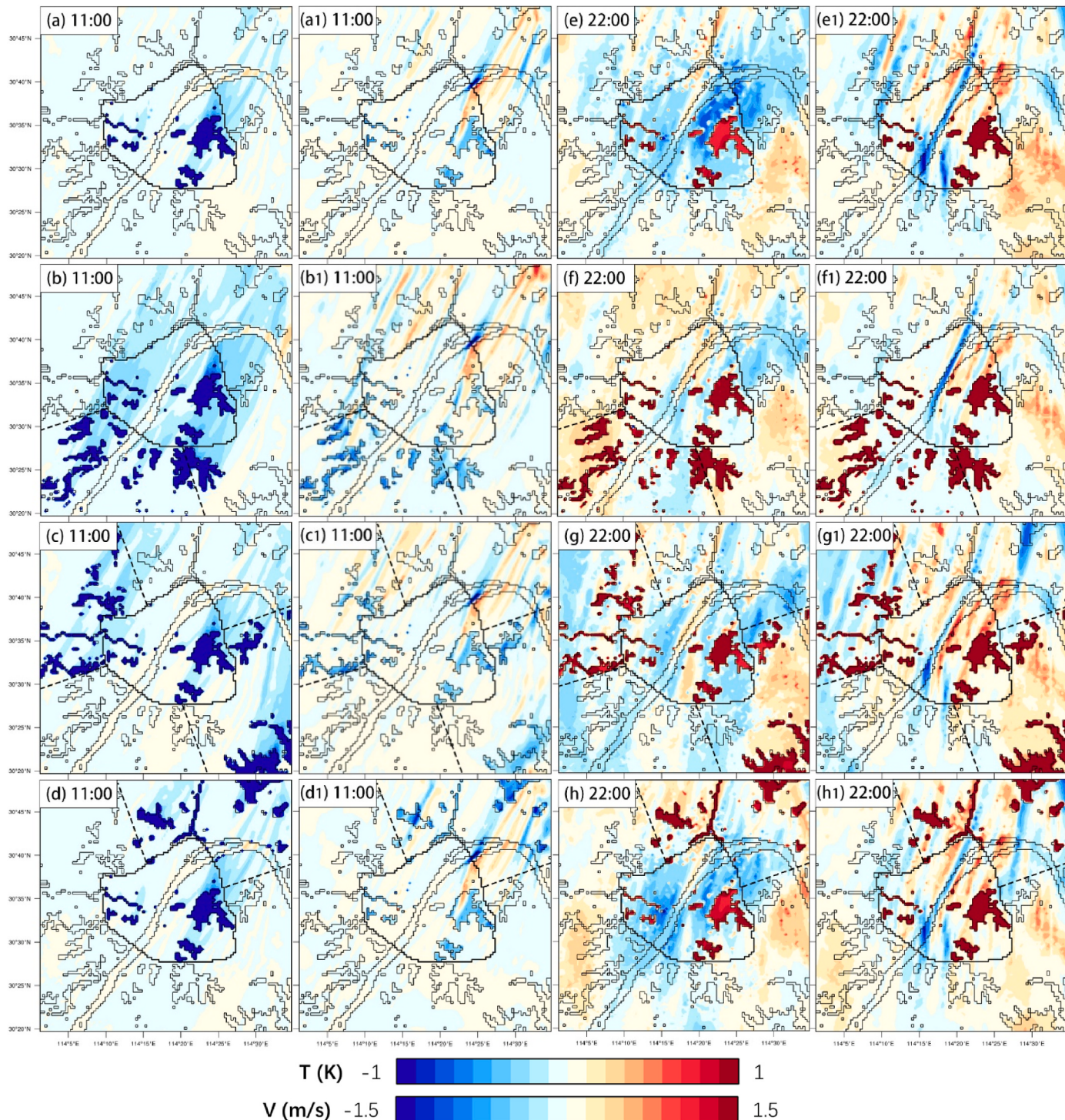


Fig. 5. Difference in air temperature at 2 m above ground (T2), wind velocity at 10 m above ground (V10) between the experimental cases (DL, UP, SIDE, DOWN), and the control case NL, (Results of Experimental case minus Control case). The data at 11:00 and 22:00 was used for analysis.
 11:00: (a) DL T2, (a1) DL V10, (b) UP T2, (b1) UP V10, (c) SIDE T2, (c1) SIDE V10, (d) DOWN T2, (d1) DOWN V10. 22:00: (e) DL T2, (e1) DL V10, (f) UP T2, (f1) UP V10, (g) SIDE T2, (g1) SIDE V10, (h) DOWN T2, (h1) DOWN V10.

speed difference shown in Fig. 5(e1)–(f1), water bodies significantly promote urban ventilation at night, which facilitates the removal of air pollutants, such as atmospheric particulates and trace gases.

The results shown in Fig. 5 are quantitatively described in Fig. 6. The statistical indicator was the average T2 above the land surface in downtown areas (i.e., the above water bodies were not considered). Consistent with Fig. 5, the result is the difference between the experimental and control cases, which shows the effect of the water body on

the air temperature. The day and night marked in the figure are distinguished by the intensity of the shortwave radiation.

First, the characteristic of the curves after sunrise (5:00) is that with the increase in background air temperature, the warming effect of water bodies at night gradually transforms into a cooling effect. In the DL, SIDE, and DOWN cases, the time point of the transformation occurred at approximately 6:30, whereas in the UP case, it occurred at 7:30. This suggests that upwind suburban water bodies delayed the reversal time

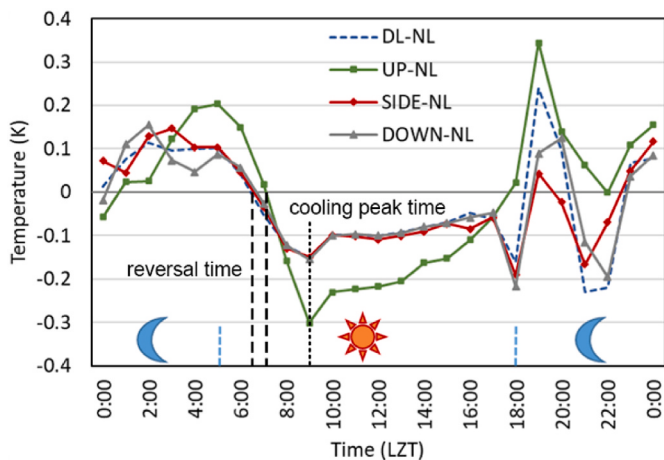


Fig. 6. Air temperature difference between the experimental cases (DL, UP, SIDE, DOWN) and the control case NL at 2 m above ground, taking the average value above land surface in downtown areas.

by approximately 1 h, implying that the intensity and duration of urban nighttime warming were greater. While upwind water bodies keep the city warmer than the average temperatures during sunrise, the cooling effect is also the greatest under rapidly rising background temperatures. After 6:00, the slope of the UP curve was significantly higher than that of the other three curves, and from 8:00, the temperature drop also exceeded that of the others. For all cases, the cooling effect of the water bodies during the day reached a maximum at 9:00, and then gradually decreased with time. The cooling peak of DL at 9:00 is 0.15 K and remained around 0.1 K during the midday period, while that of UP is almost twice as high.

The complexity at night can also increase. Between 18:00 and 20:00, the rapid weakening of solar radiation induced a rapid drop in the

surface temperature, and the water bodies significantly reduced the cooling rate of urban areas. Between 21:00 and 22:00, after the cooling trend caused by the disappearance of solar radiation stabilized, water bodies still had a cooling effect on urban land surfaces. However, the abnormal cooling effect increases at 18:00 in cases DL, SIDE, and DOWN, which cannot be explained by the observations. Nonetheless, the existence of upwind suburban water bodies makes the transformation between cooling and warming relatively stable during the sunset. In addition, upwind suburban water bodies warm downtown areas during evening hours. This additional heating effect can reach a maximum of nearly 0.3 K between 21:00 and 22:00 (comparing the UP and DL curves), which essentially offsets the cooling effect accumulated during the day. Regarding the mean value, the downwind and east-west sides of suburban water bodies have no significant effect on the thermal environment in downtown areas at night. In Fig. 5h, suburban water bodies in the downwind area reduce the temperature in the west but increase it in the east, which is not reflected in the mean value.

3.2. Impact of water bodies on the vertical distribution of air temperature and wind speed

In Section 3.1, we found that the lake breeze circulation promotes air movement in the vertical direction, which also plays an important role in the evacuation of heat within the urban canopy. Moreover, suburban water bodies located in different regions may have different effects on vertical movement. Therefore, the vertical distributions of the air temperature and wind speed over the downtown area were explored. We considered downtown as the horizontal boundary and extracted the air temperature data of each vertical layer (16 layers within 2 km of the ground) for 25 h (0:00–24:00, UTC+8). The average air temperature of all grids in each vertical layer was then calculated and plotted in Fig. 7 using the interpolation method to represent the variation in the average air temperature downtown with time and height. The value in Fig. 7 is the difference between the experimental and control case NL to reflect

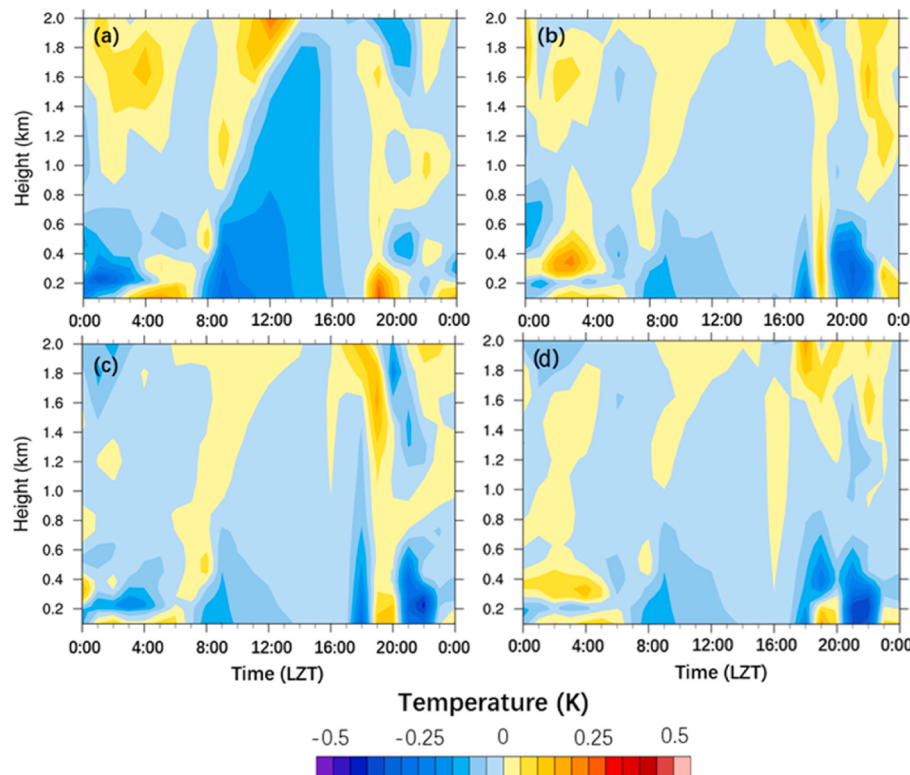


Fig. 7. Effect of water bodies on the average air temperature in downtown areas varies with time and height. (a) UP, (b) SIDE, (c) DOWN, (d) DL. The value is the result of the experimental cases minus the control case.

the impact of the water bodies.

First, as shown in Fig. 7, during the day, between 7:00 and 19:00, water bodies in each area lower the average temperature over the city but increase the temperature in the upper areas. During the day, between 7:00 and 19:00, water bodies lowered the air temperature near the land surface in all cases, but increased the air temperature in the upper air. The temperature drop was largest in the morning (8:00–12:00) when the background temperature increased rapidly, and the maximum height of the cooling effect occurred in the afternoon when the air temperature was the highest (14:00–15:00). The results show that, owing to the presence of water bodies, part of the heat from the urban surface is transferred to the upper air. Thus, the lake breeze circulation may promote heat evacuation in the vertical direction. Therefore, the specific development of the lake breeze circulation was analyzed using the profile shown in Fig. 9. However, it is worth noting that in the temporal dimension, the development of a temperature drop near the land surface was not synchronized with that of the vertical range of the cooling effect. Consistent with the results in Fig. 6, the temperature drop caused by the water bodies reached a peak value at 9:00, but not in the afternoon when the background temperature and lake-land temperature difference were the highest. Next, in Fig. 7a, suburban water bodies upwind show the most obvious cooling effect on the lower atmosphere above downtown. The drop in temperature near the land surface can reach up to 0.3 K at around 9:00, and there is still a relatively cooling effect at the highest altitude of 1.8 km. The cooling effect was much stronger than that in the DL case, where the downtown water bodies acted alone (Fig. 7d). Accordingly, the synergistic effect of suburban water bodies upwind and in downtown areas may enhance lake breeze circulation and increase the heat transported vertically, thus significantly reducing the temperature of the urban ground. This speculation is verified in Fig. 9.

In the evening hours (20:00–23:00), for the DL, SIDE, and DOWN cases (Fig. 7a and d), water bodies bring a significant cooling effect (0.1–0.4 K) to the space below 600 m. However, in the UP case, this cooling effect is hardly visible. Therefore, this may indicate that the warm air brought by upwind suburban water bodies not only significantly affects the thermal environment near the surface (Section 3.1), but also raises the air temperature within several hundred meters of vertical height.

To verify whether lake breeze circulation promotes vertical heat

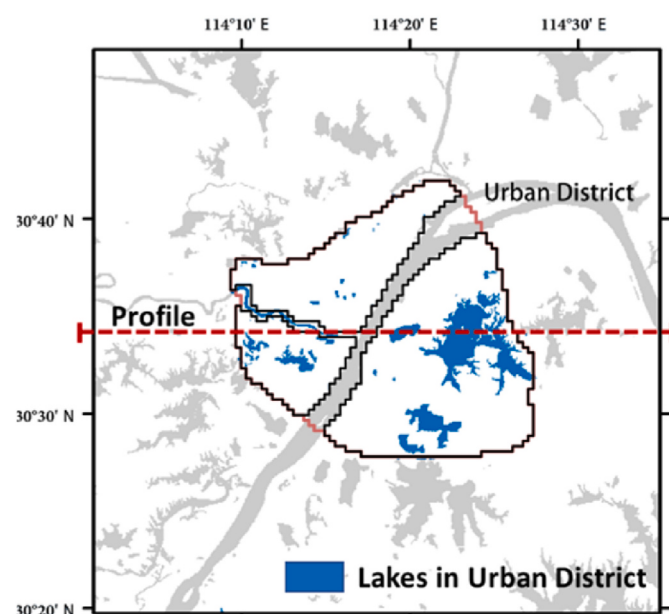


Fig. 8. Schematic diagram of profile.

transport, the vertical distribution of air temperature and vector wind speed was studied. The location of the profile is shown in Fig. 8, which is a longitudinal section, is shown in Fig. 8. To better observe the interaction between lake breeze circulation and urban areas, the profile was set at a position passing through the center of Wuhan and across the three lakes on the east side. Fig. 9 shows the distribution of air temperature and vector wind speed at 11:00. The results show the difference between the experimental cases and the control case NL. A profile schematic is placed below the image for spatial reference, and the triangular signs on the horizontal axis mark the boundary position downtown.

First, from the results of the DL case in Fig. 9d, in the eastern region, vertical local circulations appeared over lakes 1 and 2, and the circulation over Lake 1 (the larger lake) was significantly stronger. The air temperature at the bottom of the circulation decreased by up to 0.5 K, while it increased by up to 0.4 K above 1.4 km above the top of the circulation. This indicates that during the day, lake breeze circulation induced by water bodies can transport surface heat to the upper air, effectively reducing heat accumulation inside the urban canopy.

Then, by comparing DL to the other three cases, when in downtown and suburban water bodies act synergistically, the intensity of local circulation is higher than when they act alone. This phenomenon was particularly evident in the UP. This is because under the action of the background wind, the abundant water bodies in the upwind suburb input a large amount of cool air near the surface of the downtown area, which enhances the thermal difference in the vertical direction and promotes the generation and development of local circulation. As shown in Fig. 9a, when upwind suburban water bodies were considered, the areas with local circulation first increased. For example, there is obvious local circulation in the west, although these areas are not directly above the water body. This is because the water bodies west of the downtown area are too small to stimulate lake breeze circulation. After many water bodies distributed in the southwestern suburbs send cold air to these areas, local circulation is generated, which is consistent with the formation mechanism of the lake breeze circulation. Second, the characteristics of the existing local circulation become clearer. The temperature drop at the bottom of the circulation above Lake 1 increases to 0.8 K and there is still a temperature drop of up to 0.4 K at 1.4 km above the ground, while the temperature rise in the upper air also increases to a maximum of 0.8 K. However, in case SIDE (Fig. 9b), water bodies have little effect on the local circulation in downtown areas, and only slightly enhance the vertical heat transport in the western and eastern suburban areas. The effect of downwind water bodies (Fig. 9c) was almost unobservable, with almost no difference from the DL case.

According to Sections 3.1 and 3.2, suburban water bodies located in the upwind direction (south side) of the downtown area show the most obvious reduction in urban daytime air temperature. Considering the hot summers and cold winters in Wuhan, water bodies in this area should be protected.

However, with the recent expansion of downtown areas, the construction intensity in the suburbs is increasing. Although urban expansion is inevitable, buildings in the upwind direction are too dense, and more heat accumulates downtown. Meanwhile, the climate regulation ability of upwind suburban water bodies may be damaged, inducing the deterioration of the downtown thermal environment. Therefore, finding a balance between urban construction and protection of the climate regulation capacity of water bodies is the next problem to be addressed.

3.3. Impact of suburban construction intensity increase on the urban thermal environment

3.3.1. Additional case settings

The capacity of suburban water bodies to affect downtown thermal environments during suburban urbanization was explored to provide a quantitative control strategy for construction intensity to maximize the climate regulation capacity of suburban water bodies downtown. The

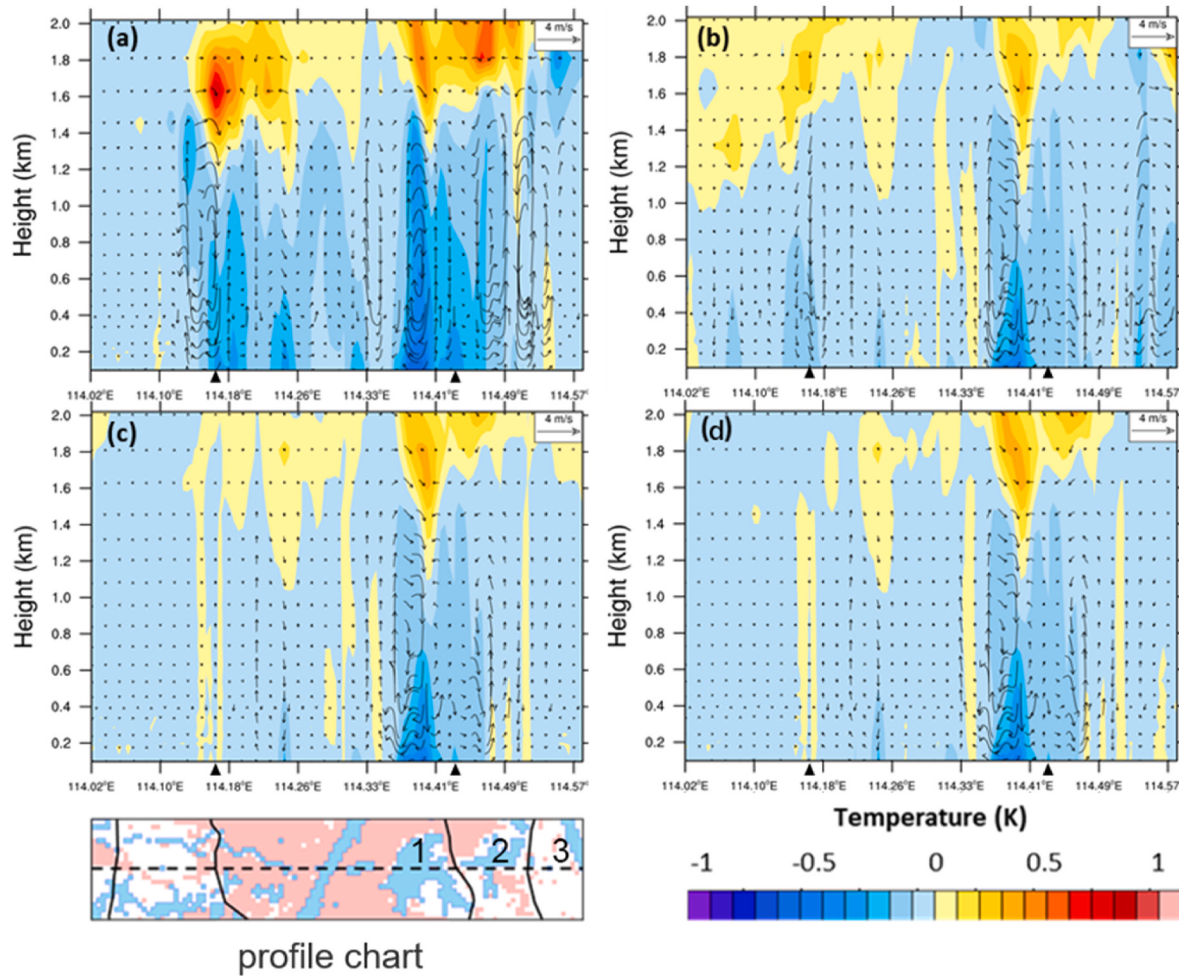


Fig. 9. Effect of water bodies on air temperature and vector wind speed at the profile at 11:00 a.m. (a) UP, (b) SIDE, (c) DOWN, (d) DL. Note: The value is the result of the experimental cases minus the control case.

increase in construction intensity is simplified as the building density increases, whereas the assumed average building height remains unchanged. Because this section focuses on the interaction between water bodies and urban forms, factors such as anthropogenic heat emissions have not yet been discussed.

Based on the results, the suburbs located southwest (upwind direction) of the downtown area were considered as the research area

(marked in yellow in Table 5), and building density and height were selected as experimental variables. We modified the source code in the UCM module to add a new city category (land-use category = 34). We then uniformly set the urban land categories in the research area to "category = 34" and clarified the UCPs dataset. Thus, the urban morphological parameters of the research area can be independently controlled by the URBPARAM.TBL input. The rest of the simulation area was equal to that of the UP case.

To represent a prototype for future construction in the suburbs, we counted the building information of all newly built areas in the southern suburbs. The statistical values of building density and average building height were 17.9% and 16.3 m, respectively. Finally, the model values of building density and average building height in the study area were set to 20% and 20 m, respectively. By increasing the building density in the upwind suburbs, the cooling effect of water bodies in the downtown area changes accordingly. The ideal reference value of suburban construction intensity can then be obtained from the above experimental conclusions. Therefore, five cases are presented in this section, as the average building height was maintained at 20 m, and the building density increased from 20% to 60% with a 10% gradient (Den1 = 20%, Den2 = 30%, Den3 = 40%, Den4 = 50%, Den5 = 60%). In addition, a corresponding control experiment was set up for each case, in which all water bodies in Wuhan were replaced with dry land while maintaining the same height and density parameters of the study area as the experimental case.

Table 5
Additional case setting.

	Experimental group		Control group		
	Den1	Den2	Den3	Den4	Den5
Density	20%	30%	40%	50%	60%
Height	20 m	20 m	20 m	20 m	20 m

3.3.2. Impact of suburban construction intensity on the distribution of heat island in downtown

Fig. 10 shows the trend of heat island intensity in downtown areas with increasing building density in the southern suburbs. The average temperature between 16:00 and 17:00, when the solar radiation gradually weakened but the urban heat accumulated significantly, was selected as the research period.

To identify areas with harsh thermal environments, the downtown areas in Fig. 10 were divided into five heat island intensity levels [40]: intense heat island ($T > U + STD$), heat island ($U + 0.5STD < T < U + STD$), normal ($U - 0.5STD < T < U + 0.5STD$), cold island ($U - STD < T < U - 0.5STD$), and intense cold island ($T < U - STD$). U and STD are the mean and standard deviation of air temperature in the study area, respectively. To directly reflect the impact of the increase in building density on the current situation, U and STD in Fig. 10a-d uniformly take the value in Den1, which represents the current city situation rather than the actual value in each case. As shown in Fig. 10, the areas with harsh thermal environments in downtown areas are mainly distributed on both sides of the Yangtze River, and these areas have the highest construction intensity and the least natural surface. Moreover, the intense heat island areas were mainly distributed north of the downtown area (marked with a black square in Fig. 10a), located in the downwind direction. The microclimate of these areas is vulnerable because the increase in urban emissions and weakening of ventilation potential aggravate the accumulation of heat and air pollution.

Comparing Fig. 10a and c, when the building density in the southern suburbs increased from 20% to 40%, the thermal environment in the downtown area did not deteriorate significantly. In cases Den1, Den2, and Den3, the intense heat island area accounted for 5.5%, 5.5%, and 4.9% of the total land area downtown, respectively. In addition, when the building density increased to 40%, although the intense heat island

areas decreased slightly, they heat island areas increased and extended to the south of the main urban area. It is likely that under the current construction intensity conditions, reasonable suburban development will not have a significant negative impact on the thermal environment of the main urban area. However, as shown in Fig. 10c and d, when the building density exceeded 40% and continued to increase, the thermal environment in the northern part of the downtown area deteriorated rapidly. In cases Den4 and Den5, the proportion of the intense heat island areas increased to 7.9% and 10.7%, respectively. When the suburban building density increases to 60% of the status, the intense heat island areas may double.

In addition, the boxplot shown in Fig. 10 shows the straight-line distance between calculation grids, which are classified as intense heat islands, and the southern border of downtown (marked with a gray dotted line), which is used to describe the spatial distribution changes of the intense heat island areas. The figure shows that first, when the building density reaches 40% and continues to increase, the distribution range of the intense heat island areas increases rapidly. Second, from the upper and lower quartiles and medians, and the increase in building density, the spatial geometric center of the intense heat island areas continues to move southward, closer to the city center. For the Den3 case, the reason for the small statistical value is that the intense heat island areas increased in the south and decreased in the north. This means that the thermal environment in the city center is most significantly affected by construction in the suburbs.

Therefore, if only the thermal environment is considered, when the building density of the southern suburbs is controlled below 40%, the negative impact on the downtown areas is insignificant. However, this result does not consider the increase in plot ratio and population density caused by the increase in building density, which is accompanied by the use of more vehicles and electrical appliances, especially air

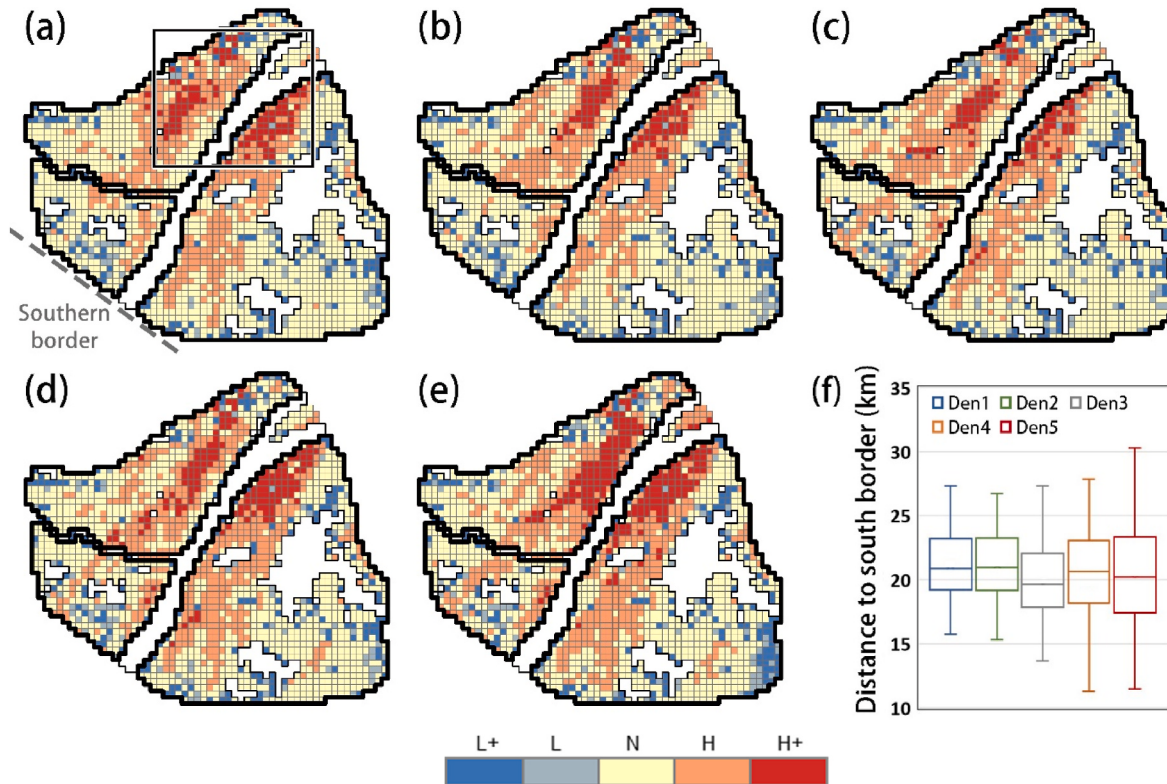


Fig. 10. Spatial distribution of heat island intensity in downtown when the suburban building density increases. (a) case Den1 (Suburban building density 20%), (b) case Den2 (Suburban building density 30%) (c) case Den3 (Suburban building density 40%), (d) case Den4 (Suburban building density 50%), (e) case Den5 (Suburban building density 60%), (f) straight-line distance between the calculation grids which are classified as intense heat island and the southern border of the downtown area.

Note: L+, intense cold island; L, cold island; N, normal; H, heat island; H+, intense heat island.

conditioners, in summer, which will result in high heat emissions. Therefore, considering the actual situation, building density in the suburbs should be controlled to a level much lower than 40%.

3.3.3. Impact of suburban construction intensity on the climate regulation capacity of water bodies

In Sections 3.1 to 3.2, we concluded that the water bodies in the southern suburbs can effectively alleviate the heat island effect in the main urban areas by inputting cold air and other means. However, with the increase in the intensity of suburban construction, what will happen to this adjustment capacity of water bodies? This is a problem that we want to be solved.

Fig. 11 shows the capacity of water bodies in the southern suburbs to affect air temperatures in the downtown area as building density increased in the southern suburbs. **Fig. 10** shows that the northern part of the downtown area had the highest heat island intensity. Therefore, we divided the downtown area into northern and southern regions (**Fig. 12f**) based on the geometric center of Wuhan, that is, the intersection of the Yangtze and Han rivers. In the data analysis, we calculated the average T2 value in the northern and southern parts of the downtown area. **Fig. 11** shows four time periods: noon (12:00–15:00) when the solar radiation is the strongest; afternoon period (16:00–17:00) when the solar radiation gradually weakens, but the urban heat accumulates at 18:00–20:00 when the temperature drops rapidly after sunset; and evening (21:00–22:00). This section focuses on the noon and afternoon periods when the cooling effect of water bodies is significant, yet the evening period when the water body acts as a heat preservation is not discussed in detail.

From **Fig. 11a** and b (12:00–15:00), the cooling effect of suburban water bodies downtown was not affected by the increase in suburban building density. This is because the background temperature is high owing to the strong solar radiation and the difficulty in reflecting the difference caused by the change in urban form.

In the afternoon (16:00–17:00), when the solar radiation gradually weakened, the impact of the increased building density in the suburbs became prominent. In the southern and northern parts of the downtown area, the cooling effect of suburban water bodies was strongest when the suburban building density was 40% (Den3) and weakest when the suburban building density was 60% (Den5). In addition, in the northern part of downtown, located downwind, the time-dependent trend of the cooling effect was delayed by approximately 1 h compared with that of the southern part, and the cooling effect was more obviously affected by the building density. Compared with the gray curves in **Fig. 11a** and b, when the solar radiation decreased sharply, the cooling effect of the water body on the southern part of downtown disappeared and became disordered at 17:00, whereas it was delayed to 18:00 in the northern part. Similarly, at the time point when the water body showed a steady warming effect at night, in the southern part, it occurred between 19:00 and 19:30, whereas in the northern part, it occurred uniformly at 20:00.

In addition, whether it is at 15:00–16:00 or 20:00–23:00, the differences among the northern parts are more obvious and regular. It is not difficult to find that the distance between the target area and the water body in the upwind suburb is an important influencing factor, that is, the background wind drives the climate influence of water bodies in upwind suburban to gradually cover the whole city from south to north, and the southern region may have acted as a buffer zone.

This further revealed an interesting phenomenon, both in terms of heat island intensity and the cooling effect of the water body. The area most affected by the construction of the southern suburbs is the northern part of the downtown area, where heat tends to accumulate, rather than the southern part that is closest to the suburbs. Therefore, it is particularly important to control the urban forms in the northern part of the city. Dense building clusters should be avoided and ventilation channels should be planned to promote natural urban ventilation.

As shown in **Fig. 11b**, for the cooling effect of the water body, Den3 (40%) \approx Den2 (30%) $>$ Den1 (20%) $>$ Den4 (50%) $>$ Den5 (60%), that is, when the building density started to increase from 20%, the cooling effect first increased with an increase in building density and then reached a peak when the density was approximately 30%–40%. Places with higher construction intensity usually have higher air temperatures, followed by greater thermal differences between lakes and land; therefore, the cold island effect of wetlands is more significant [18]. Subsequently, as the building density increased, the cooling capacity of the water body decreased rapidly.

Fig. 12a–e shows the effect of increasing building density on the cooling effect of water bodies at 17:00. In cases Den2 and Den3, the cooling effect of suburban water bodies on downtown is stronger than that of Den1. In case Den2, many regions with a cooling range of about 0.3 K appear in the northwest; in Den3, the cooling effect in the northeast region is significantly enhanced. When the building density increases to more than 50%, in cases Den4 and Den5, the cooling effect brought by water bodies is greatly weakened in both coverage area and temperature drop. At this time, the climate regulation effect of suburban water bodies to downtown is almost completely invisible. When combining **Figs. 11a** and **12e**, the building density reaches 60%, water bodies significantly increase the temperature in the southern part of downtown, and the increase can reach 0.5 K. This may imply that the high building density in the suburb not only hinders the penetration of cool air from suburban water bodies into downtown, but also increases the heat input from the suburb to downtown due to the local circulation formed by the suburban water bodies and dense buildings in the suburb.

In the evening (21:00–22:00), after the average building density exceeded 40% (cases Den4 and Den5), the effect of the water bodies on increasing air temperature also increased (**Fig. 11b**). In the northern part of downtown, Den5 (60%) showed the largest temperature rise, while Den4 (50%) ranked second, which is not conducive to the mitigation of urban heat islands.

Thus, in future urban construction, the average building density

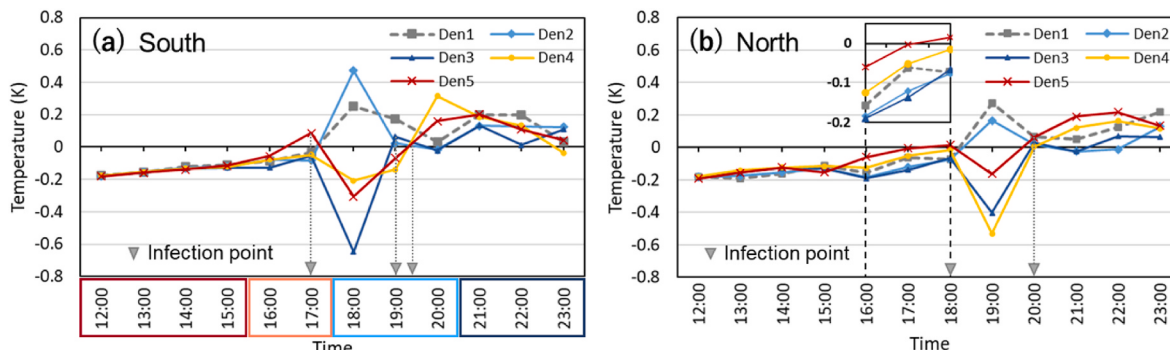


Fig. 11. T2 difference between the experimental and their control cases (Experimental case – Control case), only air temperature over land is extracted. (a) Take the average air temperature in the southern area of downtown, (b) the average air temperature in the northern area of downtown.

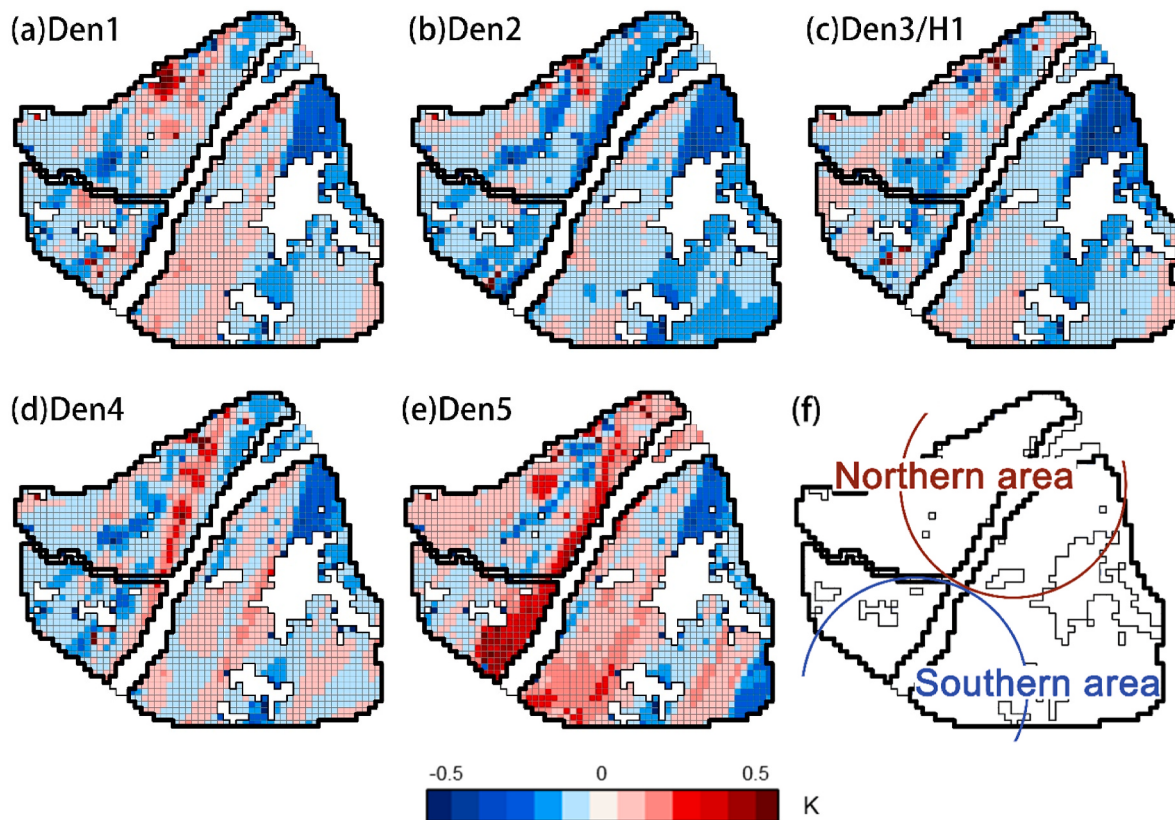


Fig. 12. Difference in T_2 between experimental cases and control cases at 17:00 (experimental case - control case) (a) Den1, (b) Den2, (c) Den3/H1, (d) Den4, (e) Den5, (f) Data extraction regions: Southern and Northern.

should be controlled within 40%. This may exert the climate regulation capacity of water bodies in the southern suburbs to alleviate the summer urban heat islands in downtown areas.

4. Discussion

The lake wind circulation formed by the temperature difference between the lake and land facilitated the evacuation of urban heat. This process can be briefly divided into two steps. First, the pressure difference causes the cool air above the lake to be transported to land, which directly reduces the urban air temperature. Second, the cool air from the lake is heated by the land surface to form a vertical upward lake breeze front. Heat and air pollutants in coastal areas enter the lake breeze circulation through the lake breeze front and are transported to the upper air [41,42]. The intensity of the lake breeze generally maintains a trend in line with changes in the background air temperature. In an observation of Taihu Lake, Qin et al. monitored the temperature difference between the lake and land, which reached 0.6 K at 9:00, and the average wind speed reached the maximum (2.1 m/s) when the temperature peaked (3.4 K) at 14:00 [43]. These results were consistent with our conclusions.

However, the development of the lake breeze intensity and the cooling effect of the water body on the near-surface air temperature do not seem to be consistent in the time dimension. To further discuss this phenomenon, the average value of T_2 above the water bodies and waterfront areas in downtown was extracted and calculated, where the waterfront area refers to the calculation grids around water bodies (grid size 500 m). The two were subtracted to obtain the temperature difference between the lake and the land, and the results are shown in Fig. 13. It can be seen from the figure that the average lake-land temperature difference reached 0.7 K at 9:00, and peaked at the same time as the background temperature (1.8 K) at 14:00. However, the cooling

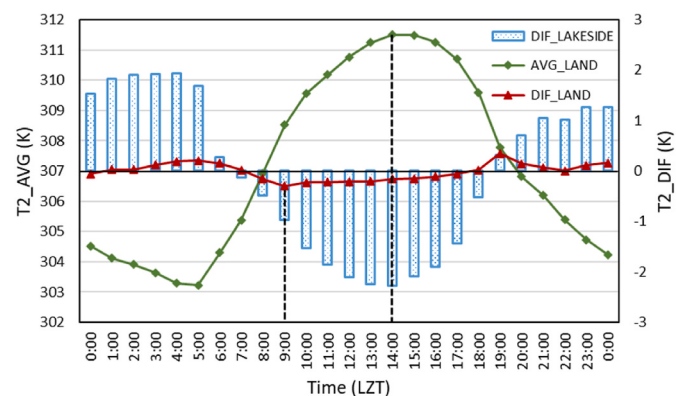


Fig. 13. Temperature difference between lake and land at 2 m above the ground in the case UP.

effect of water bodies downtown reached a peak of 0.3 K at 9:00 and continued to decrease as the temperature increased between 9:00 and 14:00.

DIF_LAKESIDE is the average temperature difference between lake and land in downtown (case UP), AVG_LAND is the average temperature of the land surface in downtown (case UP), and DIF_LAND represents the average temperature drop brought by water bodies on the land area of downtown (result of case UP - case NL).

Why are both the lake-land temperature difference and intensity of the lake breeze increasing, while the cooling effect of water bodies is constantly weakening? To answer this question, we selected three time periods (9:00, 11:00, and 14:00) to observe the impact of the water body on the vector wind speed in the profile (Fig. 8). At 9:00, local circulation can be observed over the water body, but the vertical velocity of air was

very low. At 11:00, the characteristics of local circulation were evident, and the vertical velocity reached 1 m/s. At 14:00, when the temperature is highest, the vertical speed exceeds 1.5 m/s (Fig. 14). This shows that, for the scattered water bodies in Wuhan, the law that the lake breeze circulation intensity is positively correlated with temperature holds true. The top height of the lake breeze circulation increased with the temperature (Fig. 14a–c). At 9:00, the upper boundary of the lake breeze circulation could not be clearly observed, and from 11:00 to 14:00, the top of the circulation rises from 1.6 km to more than 2 km. Wang et al. also found that in Taihu Lake, from the early morning to noon, ozone rose to 2 km under the lift of the lake breeze front and then accumulated

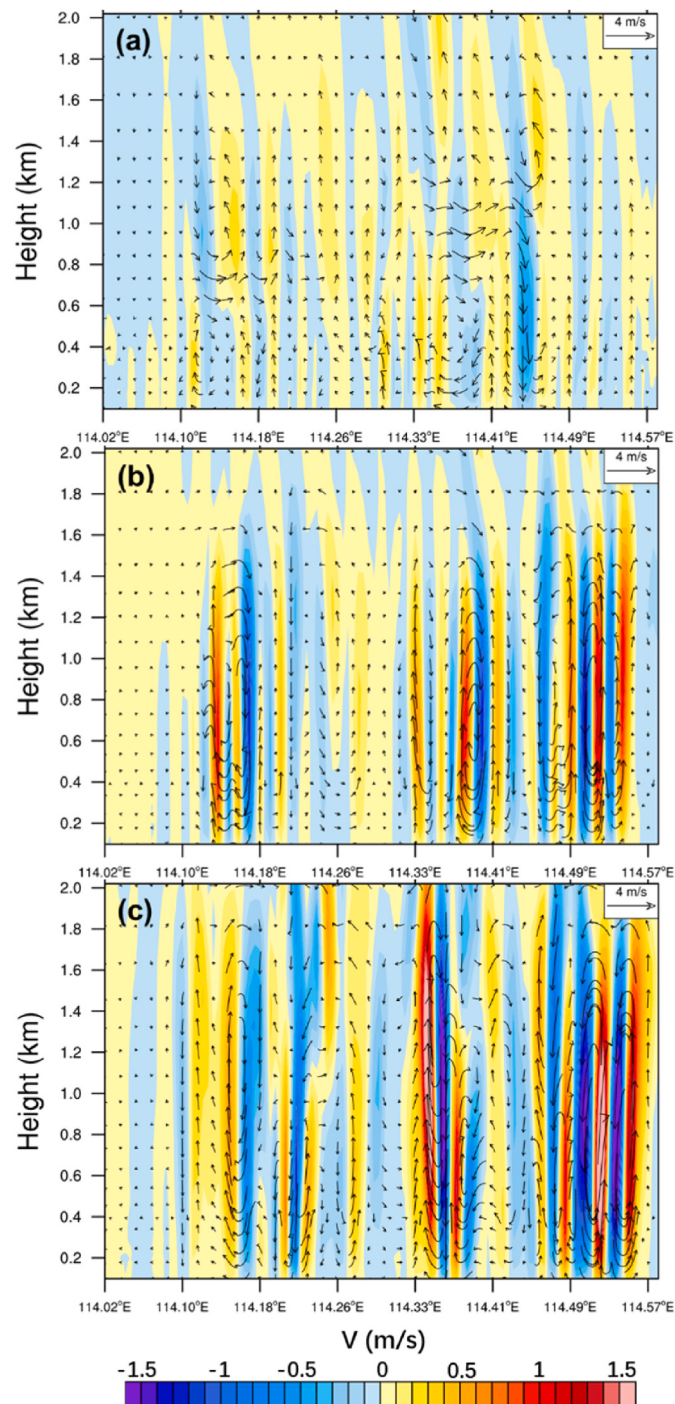


Fig. 14. Vertical wind speed difference between the UP case and the NL case at the profile (a) 9:00, (b) 11:00, and (c) 14:00.

there [44].

As shown in Fig. 7a, the maximum height of the water body required to produce the cooling effect increased continuously from 8:00 to 15:00. Combining the two, it is reasonable to speculate that when the background air temperature increases, the sensible heat and latent heat exchange brought about by the water body will indeed increase (under the premise that the change in water surface temperature is negligible). However, the increase in the lake-land temperature difference also causes the lake breeze circulation to develop rapidly in the three-dimensional direction, so the increase rate of heat exchange cannot catch up with the expansion rate of the action range. Therefore, the more developed the lake wind circulation, the higher the cooling effect of water bodies can extend vertically, which leads to a reduction in the total heat in the lower atmosphere; however, the cooling effect on the urban surface is relatively weakened.

Owing to space limitations, a demonstration of this speculation will be carried out in future research. In addition, the heat loss of a city due to lake breeze circulation was calculated for existing water bodies and cities. Furthermore, the heat transported to the upper air affects the vertical structure of the atmosphere during the day and night, and whether it affects the formation of an inversion layer or rainfall [45] and the quantitative relationship between the scale of lake breeze circulation and construction intensity of the waterfront area will be assessed.

5. Conclusion

This study produced a UCPs dataset based on building information from Wuhan in 2018 and built a UCP-based single-layer urban canopy model. After verifying the validity of the model, the impact of the water bodies across Wuhan on the thermal environment of the downtown area during hot summers was explored. The main conclusions are as follows.

- (1) During the day, the suburban water bodies located upwind (south) of downtown show the most significant reduction effect on the air temperature 2 m above the ground in downtown. At 11:00, these water bodies bring an additional cooling of more than 0.1 K in average in downtown and 0.4 K in local areas. Suburban water bodies located on east-west sides and downwind directions have little effect.
- (2) During the day, water bodies promote the evacuation of heat inside the urban canopy to the upper air by enhancing the lake breeze circulation. Moreover, when water bodies in the upwind suburbs and downtown areas acted together, both the scale and wind speed of the lake breeze circulation increased significantly. At 11:00, the temperature drop at the bottom of the lake breeze circulation increases from 0.5 K to 0.8 K, with a temperature drop of up to 0.4 K at 1.4 km above the ground, while the temperature rise in the upper air also increases to a maximum of 0.8 K.
- (3) The development of the lake breeze intensity and the cooling effect of the water body on the near-surface air temperature do not seem to be consistent in the time dimension. The average lake-land temperature difference reaches 0.7 K at 9:00, and peaks at the same time as the background temperature (1.8 K) at 14:00. However, the cooling effect of water bodies downtown reached a peak of 0.3 K at 9:00 and continued to decrease as the temperature increased from 9:00 to 14:00. This may be because the rate of increase in heat exchange cannot keep up with the rate of expansion of the action range; therefore, the reduction in the total heat in the lower atmosphere, although the cooling effect on the urban surface, is relatively weakened.
- (4) Water bodies in upwind suburbs warm downtown areas during the evening hours. This additional heating effect can reach a maximum of nearly 0.3 K between 21:00 and 22:00, which basically offset the cooling effect accumulated during the day. However, the warming effect of water bodies located on the east-west side and downwind direction was not obvious.

- (5) As the building density in the southern suburbs increased from 20% to 40%, the thermal environment in the downtown area did not change significantly. However, when it continued to increase to 50% and 60%, the proportion of intense heat island areas downtown increased rapidly from 5.5% to 7.9% and 10.7%, respectively. With an increase in building density in the suburbs, the intense heat island areas north of the city gradually expanded to the city center.
- (6) Densification of suburban buildings has a significant impact on the climate regulation capacity of suburban water bodies. When the building density increased from 20% to 30–40%, the cooling effect of suburban water bodies increased slightly. However, it rapidly decreased when the building density increased from 40% to 60%.

This study has several limitations. First, optimizing the input of thermal parameters in the UCP-based urban canopy model remains an urgent problem that needs to be solved. In the evening hours, heat in the urban canopy is mainly generated by buildings during the day and by anthropogenic heat emissions. Therefore, accurate measurement of these parameters is crucial for studying the development of urban heat islands at night. Second, owing to the lack of high-altitude observational data in the discussion of lake breeze circulation, this study cannot fully demonstrate the principle of interaction between lake breeze circulation and the cooling effect of water bodies on the near-surface air temperature. We will attempt to solve these problems and hope to communicate and cooperate with researchers by focusing on related issues.

CRediT authorship contribution statement

Dun Zhu: Writing – review & editing, Writing – original draft, Visualization, Validation, Software, Methodology, Formal analysis, Data curation. **Xuefan Zhou:** Supervision, Project administration, Investigation, Funding acquisition. **Wei Cheng:** Validation, Visualization.

Declaration of competing interest

The authors declare that they have no known competing financial interests or personal relationships that could have appeared to influence the work reported in this paper.

Data availability

Data will be made available on request.

Acknowledgements

This work was supported by the National Natural Science Fund Youth Project (Grant No. 51708237), the Independent Innovation Fund of Huazhong University of Science and Technology (Grant No. 2172019kfYXKJC057). In addition, we would like to thank Editage (www.editage.cn) for English language editing.

References

- [1] M.X. Zhang, Y. Zhou, J.J. Cao, G.P. Cao, Q.Q. Ye, Analysis of spatial and temporal changes of ecological land use in Wuhan City from 2000 to 2015, *Chinese J. Agric. Res. Reg. Plan.* 42 (2021) 168–177, 01.
- [2] S. Weber, K. Kordowski, W. Kuttler, Variability of particle number concentration and particle size dynamics in an urban street canyon under different meteorological conditions, *Sci. Total Environ.* 449 (2013) 102–114.
- [3] C.P. Hou, J.W. Hou, Q. Kang, X. Meng, D. Wei, Z.A. Liu, L.L. Zhang, Research on urban park design combined with the urban ventilation system, *Cleaner Energy Cleaner Cities* 152 (2018) 1133–1138.
- [4] R. Kress, Regionale Luftaustauschprozesse Und Ihre Bedeutung Ffir Die Raumliche Olanung, Institut fur Umweltschutz Der Universität Dortmund, Dortmund, 1979, pp. 154–168.
- [5] Q.H. Weng, H. Liu, B.Q. Liang, D.S. Lu, The spatial variations of urban land surface temperatures: pertinent factors, zoning effect, and seasonal variability, *IEEE J. Sel. Top. Appl. Earth Obs. Rem. Sens.* 1 (2) (2008) 154–166.
- [6] L.H. Xu, W.Z. Yue, A study on thermal environment effect of urban park landscape, *Acta Ecol. Sin.* 28 (4) (2008) 1702–1710.
- [7] J.M. Keeler, D.A.R. Kristovich, Observations of urban heat island influence on lake-breeze frontal movement, *J. Appl. Meteorol. Climatol.* 51 (4) (2012) 702–710.
- [8] Y. Hu, J.G. Tan, S. Grimmond, X.Y. Ao, Y.F. Yan, D.W. Liu, Observed and modeled urban heat island and sea-breeze circulation interactions: a shanghai case study, *J. Appl. Meteorol. Climatol.* 61 (2) (2022) 239–259.
- [9] J.B. Yang, H.N. Liu, S. Fei, N. Zhang, W.M. J, The impact of urbanization on the urban heat island in Suzhou under the influence of Taihu lake-land breeze, *J. Meteorol. Sci.* 33 (2013) 473–484, 05.
- [10] H.Y. Du, X.J. Song, H. Jiang, Z.H. Kan, Z.B. Wang, Y.L. Cai, Research on the cooling island effects of water body: a case study of Shanghai, China, *Ecol. Indicat.* 67 (2016) 31–38.
- [11] S.J. Wu, H. Yang, P. Luo, C.A. Luo, H.L. Li, M. Liu, Y. Ruan, S.J. Zhang, P. Xiang, H. H. Jia, The Effects of the Cooling Efficiency of Urban Wetlands in an Inland Megacity: A Case Study of Chengdu, Southwest China, 2021, p. 204.
- [12] P. Ji, C.Y. Zhu, Y.Y. Sheng, Effects of urban wetlands with different shapes on the temperature and humidity of ambient environment, *Chin. J. Appl. Ecol.* 28 (2017) 3385–3392, 10.
- [13] X.F. Zhou, S. Zhang, D. Zhu, Impact of urban water networks on microclimate and PM2.5 distribution in downtown areas: a case study of Wuhan, *Build. Environ.* (2021) 203.
- [14] C.W. Liu, F.Y. Zhao, G.B. Yang, Research on multiple circulations co-driven by lake breeze and urban heat islands in inner cities, *China Environ. Sci.* 39 (5) (2019) 1890–1898.
- [15] X. Ren, Y.W. Wang, Z. Zhang, Y.C. Yang, C. Hu, H.Q. Kang, Simulation studies for Lake Taihu effect on surrounding cities thermal environment, *Acta Meteorol. Sin.* 75 (4) (2017) 645–660.
- [16] E.T. Crosman, J.D. Horel, Sea and lake breezes: a review of numerical studies, *Boundary-Layer Meteorol.* 137 (1) (2010) 1–29.
- [17] D.M.L. Sills, J.R. Brook, I. Levy, P.A. Makar, J. Zhang, P.A. Taylor, Lake breezes in the southern Great Lakes region and their influence during BAQS-Met 2007, *Atmos. Chem. Phys.* 11 (15) (2011) 7955–7973.
- [18] P. Ji, X.L. He, T. Zhang, H.Y. Wang, F.J. Yang, N. Wang, Y.H. W, Effect of urban wetlands in different positions on the temperature and humidity of ambient environment in process of urbanization, *J. Heilongjiang Bayi Agric. Univ.* 31 (2019) 1–8+21, 03.
- [19] H. Wu, H. Li, H. Chen, X. Jian, The impact of Water Distribution on urban land surface temperature, *J. Mudanjiang Normal Univ.* 4 (2016) 54–57.
- [20] T.L. Zhai, J. Wang, Y. Fang, J.J. Liu, L.Y. Huang, K. Chen, C.C. Zhao, Identification and prediction of wetland ecological risk in key cities of the Yangtze River economic belt: from the perspective of land development, *Sustainability* 13 (1) (2021) 411.
- [21] C. You, J.C.H. Fung, W.P. Tse, Response of the sea breeze to urbanization in the pearl river delta region, *J. Appl. Meteorol. Climatol.* 58 (7) (2019) 1449–1463.
- [22] Y.J. Chen, H. Chen, Y.G. Guan, J.N. Wu, The spatial form control based on penetration capability of river wind: taking the enclosure pattern and street direction as an example, *Huazhong Archit.* 38 (10) (2020) 22–27.
- [23] X.Y. Wang, S.G. Miao, H.N. Liu, J.N. Sun, N. Zhang, J. Zou, Assessing the impact of urban hydrological processes on the summertime urban climate in nanjing using the WRF model, *J. Geophys. Res. Atmos.* 124 (23) (2020) 12683–12707.
- [24] S.J. Mo, S.Y. Shen, Q.L. Liao, Landscape design strategy of ventilation corridor in the green heart of CZT urban agglomeration based on WRF model, *Chinese Landscape Architect.* 37 (1) (2021) 80–84.
- [25] X.F. Zhou, H. Chen, Y.G. Guan, Study of urban ventilation corridor planning method based on a case study of Guiyang, China, *J. Human Settlements West China* 30 (2015) 13–18, 06.
- [26] F. Chen, M. Tewari, H. Kusaka, Current Status of Urban Modeling in the Community Weather Research and Forecast (WRF) Model. Joint with Sixth Symposium on the Urban Environment and AMS Forum: Managing Our Physical and Natural Resources: Successes and Challenges, Amer. Meteor. Soc. CD-ROM, Atlanta, GA, USA, 2006, J1.4.
- [27] J. Ching, M. Brown, S. Burian, National urban database and access portal tool, *Bull. Am. Meteorol. Soc.* 90 (8) (2009) 1157–1168.
- [28] F. Chen, H. Kusaka, R. Bornstein, The integrated WRF/urban modeling system: development, evaluation, and applications to urban environmental problems, *Int. J. Climatol.* 31 (2011) 273–288.
- [29] E.A. Hendricks, J.C. Knievel, Y. Wang, Addition of multilayer urban canopy models to a nonlocal planetary boundary layer parameterization and evaluation using ideal and real cases, *J. Appl. Meteorol. Climatol.* 59 (8) (2020) 1369–1392.
- [30] E. Coniglio, P. Monti, G. Leuzzi, A. Cantelli, A three-dimensional urban canopy model for mesoscale atmospheric simulations and its comparison with a two-dimensional urban canopy model in an idealized case, *Urban Clim.* 37 (2021).
- [31] E.A. Hendricks, J.C. Knievel, D.S. Nolan, Evaluation of boundary layer and urban canopy parameterizations for simulating wind in miami during hurricane irma (2017), *Mon. Weather Rev.* 149 (7) (2021) 2321–2349.
- [32] F. Salamanca, A. Martilli, M. Tewari, F. Chen, A study of the urban boundary layer using different urban parameterizations and high-resolution urban canopy parameters with WRF, *J. Appl. Meteorol. Climatol.* 50 (5) (2011) 1107–1128.
- [33] Wuhan Water Resources Bulletin, 2017.
- [34] Y.Y. Chen, X.L. Ke, F. Liu, M. Min, The area, distribution and changes of wetlands in Wuhan City in four periods since 1987, *Wetland Sci.* 17 (2019) 553–558, <https://doi.org/10.13248/j.cnki.wetlandsci.2019.05.008>, 05.

- [35] R.H. Sun, A.L. Chen, L.D. Chen, Y.H. Lu, Cooling effects of wetlands in an urban region: the case of Beijing, *Ecol. Indicat.* 20 (2012) 57–64.
- [36] Z.S. Xue, G.L. Hou, X.S. Zhang, X.G. Lyu, M. Jiang, Y.C. Zou, X.J. Shen, J. Wang, X. H. Liu, Quantifying the cooling-effects of urban and peri-urban wetlands using remote sensing data: case study of cities of Northeast China, *Landsc. Urban Plann.* 182 (2019) 92–100.
- [37] X.C. Song, J. Liu, Y. Zhao, Influence of district morphology on the thermal environment in waterfront areas in the north, *Build. Sci.* 35 (10) (2019) 191–198.
- [38] X. Zhang, G.J. Steeneveld, D. Zhou, R.J. Ronda, C.J. Duan, S. Koopmans, A.A. M. Holtslag, Modelling urban meteorology with increasing refinements for the complex morphology of a typical Chinese city (Xi'an), *Build. Environ.* (2020) 182.
- [39] P. Gong, X.C. Li, J. Wang, Y.Q. Bai, B. Cheng, T.Y. Hu, X.P. Liu, B. Xu, J. Yang, W. Zhang, Annual maps of global artificial impervious area (GAIA) between 1985 and 2018, *Rem. Sens. Environ.* (2020) 236.
- [40] Y.J. Chen, S.X. Yu, Impacts of urban landscape patterns on urban thermal variations in Guangzhou, China, *Int. J. Appl. Earth Obs. Geoinf.* 54 (2017) 65–71.
- [41] Y.F. Zhou, H.D. Guan, C.Y. Huang, L.L. Fan, S. Gharib, O. Batelaan, C. Simmons, Sea breeze cooling capacity and its influencing factors in a coastal city, *Build. Environ.* (2019) 166.
- [42] Z.Y.W. Davis, D.M.L. Sills, R. McLaren, Enhanced NO₂ and aerosol extinction observed in the tropospheric column behind lake-breeze fronts using MAX-DOAS, *Atmos. Environ.* 5 (2020).
- [43] H.R. Qin, S.D. Liu, Y.W. Wang, Analysis of a lake Taihu breeze case, *Sci. Technol. Eng.* 15 (20) (2015) 193–200.
- [44] F. Wang, Q. Li, Y.W. Wang, Lake-atmosphere exchange impacts ozone simulation around a large shallow lake with large cities, *Atmos. Environ.* (2021) 246.
- [45] Y. Xing, J.H. Liu, G.H. Ni, Impacts of urban canopy roughness on storm evolution and rainfall area, *J. Tsinghua Univ. (Sci. Technol.)* 60 (10) (2020) 845–854.